SCIENTIFIC REPORTS

nature research

OPEN

Quantifying Microsecond Exchange in Large Protein Complexes with Accelerated Relaxation Dispersion Experiments in the Solid State

Received: 15 January 2019
Accepted: 16 July 2019
Published online: 31 July 2019

Carl Öster, Simone Kosol & Józef R. Lewandowski

Solid state NMR is a powerful method to obtain information on the structure and dynamics of protein complexes that, due to solubility and size limitations, cannot be achieved by other methods. Here, we present an approach that allows the quantification of microsecond conformational exchange in large protein complexes by using a paramagnetic agent to accelerate ^{15}N $R_{1\rho}$ relaxation dispersion measurements and overcome sensitivity limitations. The method is validated on crystalline GB1 and then applied to a >300 kDa precipitated complex of GB1 with full length human immunoglobulin G (IgG). The addition of a paramagnetic agent increased the signal to noise ratio per time unit by a factor of 5, which allowed full relaxation dispersion curves to be recorded on a sample containing less than 50 μg of labelled material in 5 and 10 days on 850 and 700 MHz spectrometers, respectively. We discover a similar exchange process across the β-sheet in GB1 in crystals and in complex with IgG. However, the slow motion observed for a number of residues in the α-helix of crystalline GB1 is not detected in the complex.

Protein dynamics play an important role in many biological processes such as enzymatic catalysis, ligand binding, or molecular recognition. Many motions implicated in these processes occur on microsecond or slower time scale and can be probed using chemical exchange based methods such as relaxation dispersion[1,2]. Applying these methods to slowly tumbling proteins and protein complexes above a few tens of kDa in solution becomes increasingly difficult due to the enhanced T_2 relaxation resulting in size dependent broadening of NMR lines. In solid-state NMR, however, line broadening is independent of the size of the system. This allows the study of biomolecules in assemblies of several hundred kDa and beyond, provided the intrinsic challenges of sensitivity and resolution can be addressed successfully[3–11]. In solids, just as in solution, chemical exchange processes can be followed by observing the effects of modulation of isotropic chemical shift. In addition, they can be monitored through the effects of modulating anisotropic interactions, e.g. modulation of dipolar couplings in near-rotary resonance relaxation dispersion experiments (NERRD)[12,13]. The combination of the two approaches can yield a detailed view of microsecond motions[12]. Previously, we have shown that we can access the protein backbone dynamics of GB1 in a >300 kDa asymmetric complex with full length immunoglobulin G (IgG) by measuring ^{15}N R_1 and $R_{1\rho}$ relaxation rates[3]. Proton detection at >50 kHz magic angle spinning (MAS) frequencies provided sufficient sensitivity enhancement to obtain data for a miniscule quantity of GB1 (~50 μg in a 1.3 mm rotor) in a reasonable timespan[4]. The strong spinning frequency dependence of ^{15}N $R_{1\rho}$[14] suggested the presence of extensive slow μs motions of GB1 in the complex with IgG that are not present in GB1 crystals[3]. Since methods such as $R_{1\rho}$ relaxation dispersion[15] rely on recording numerous 2D (or 3D) spectra to measure $R_{1\rho}$ relaxation rates at several different spin lock fields, they require unpractically long experimental times for large complexes (estimated to be on the order of one to two months of experimental time for our samples). This forced us to resort to more approximate, qualitative methods to detect the presence of microsecond exchange. However, the microsecond exchange detected in this way could not account for the observed spinning frequency dependence of $R_{1\rho}$ and suggested the presence of an overall motion of GB1 in the complex[3]. To permit quantification of microsecond exchange through relaxation dispersion measurements on large protein complexes in more realistic time frames, we propose to add paramagnetic relaxation enhancement agents to the samples to accelerate ^{15}N $R_{1\rho}$ relaxation dispersion measurement. The

Department of Chemistry, University of Warwick, Gibbet Hill Road, Coventry, CV4 7AL, UK. Correspondence and requests for materials should be addressed to J.R.L. (email: j.r.lewandowski@warwick.ac.uk)

addition of a paramagnetic agent such as copper ethylenediaminetetraacetate (CuEDTA) or gadolinium diethylenetriaminepentaacetic acid bismethylamide (Gd(DTPA-BMA)), shortens ^{1}H T_1's to allow fast recycling of the experiments. This effect is frequently used in solid state NMR to speed up acquisition for chemical shift assignments and structure calculations[4,16–30].

Since the paramagnetic agent also affects ^{1}H and ^{15}N R_2's ($R_2 = 1/T_2$), its concentration needs to be adjusted to avoid excessive line broadening (see Supplementary Fig. S1 for examples of line broadening after addition of Gd(DTPA-BMA)). Generally, due to the distance dependence of the paramagnetic effect, the presence of a paramagnetic agent is not desirable in experiments for quantifying site-specific dynamics from relaxation rates. However, the exchange contribution to R_2 or $R_{1\rho}$, which is the source of relaxation dispersion related to modulation of isotropic chemical shifts (or from anisotropic interactions in NERRD experiments)[2,15], is not affected by the paramagnetic relaxation enhancement (provided it does not induce paramagnetic shifts). Thus, in principle, quantitative relaxation dispersion can still be measured in the presence of paramagnetic agents. The only difference between a relaxation dispersion experiment in the presence and absence of paramagnetic dopants should be a different base/plateau relaxation rate ($R_{1\rho,0}$). While this manuscript was in preparation, a similar approach was used to characterize exchange in crystalline SH3[31,32] but to the best of our knowledge, no extensive validation of it has been performed. Thus, to validate the proposed accelerated relaxation dispersion method, we first compared ^{15}N $R_{1\rho}$ relaxation dispersion experiments with and without paramagnetic agent on crystalline GB1 (in the following we refer to such samples as $GB1_{pre}$ and $GB1_{dia}$, respectively). Subsequently, we applied the validated technique to obtain site specific information on microsecond conformational exchange of GB1 in the >300 kDa complex with IgG.

Results

We chose Gd(DTPA-BMA) as paramagnetic dopant over the, in solid state NMR, more popular CuEDTA because Gd(DTPA-BMA) is a more inert probe. The overall negatively charged CuEDTA has in some instances been reported to bind specifically to proteins[33,34] or even disrupt assembly of certain systems (T. Polenova – private communication). The absence of any chemical shift changes in either crystalline GB1 or precipitated GB1:IgG complex upon addition of Gd(DTPA-BMA) indicates that the dopant does not interact specifically with our samples (see also Supplementary Fig. S1).

To determine the optimal concentration of the dopant, we have examined a number of samples with varying concentrations of Gd(DTPA-BMA). The optimal concentration of paramagnetic compound that results in the best compromise between shortening of ^{1}H T_1 and resolution was determined experimentally for each system. The overall broadening seems to be dependent on the specific assemblies (or rather the specific pattern of solvent accessibility). For example, 5 mM Gd(DTPA-BMA) induced levels of broadening acceptable for site specific analysis in the GB1:IgG complex but caused too much broadening in crystalline GB1 (see Supplementary Fig. S1). Paramagnetic doping may also affect the efficiency of the polarization transfer steps and lead to loss of signal. Consequently, we have also compared the overall sensitivity per unit time for each sample. Higher concentrations (2–5 mM) of Gd(DTPA-BMA) gave similar signal to noise ratios (SNRs) per unit time for GB1:IgG corresponding to an increase of approximately 5 times compared to a sample without Gd(DTPA-BMA) (see Supplementary Table S1 for a comparison of SNRs). Similar concentrations of the dopant resulted in severe line broadening for crystalline GB1, suggesting that the optimal concentration for crystalline GB1 samples is most likely less than 2 mM.

Relaxation dispersion measurements in the solid state can contain contributions from both, incoherent effects originating from dynamic processes and coherent effects originating from dipolar couplings that are not completely averaged by magic angle spinning[35]. Consequently, in order to obtain quantitative relaxation dispersion measurements, the experiments need to be performed under conditions where coherent effects are suppressed[35,36]. For ^{15}N measurements, this is typically achieved by deuteration of the studied protein and partial re-protonation at exchangeable sites and application of fast, >40 kHz, spinning[15]. For larger concentrations of remaining protons in the sample, faster spinning frequencies need to be employed. Here, we apply 60 kHz MAS to 100% back-exchanged perdeuterated [U-^{13}C,^{15}N]GB1 samples. As can be seen by the flat dispersion curves for residues not undergoing conformational exchange (see Supplementary Figs S2–7 for plots of $R_{1\rho}$ as a function of spin-lock frequencies for all samples), the dipolar dephasing is sufficiently suppressed under these conditions. Generally, residues that show clear relaxation dispersion in experiments with Gd(DTPA-BMA), exhibit the same behavior in control experiments without paramagnetic dopant (see Supplementary Fig. S8; note that some residues had to be excluded from the analysis if their peaks were heavily overlapped). We observed dispersion in two regions in crystalline GB1: the α-helix (α-helix region, residues 24, 26, 28, 29, 32, 33, 35, 36 in $GB1_{pre}$) and strands 2–4 of the β-sheet and the loops connecting them (β-sheet region; residues 12, 17–18, 44–46, 49–53 in $GB1_{pre}$). For some residues, raised rates were observed near spin locks ~5 kHz (3.14×10^4 rad s^{-1}), e.g. in D46 (Fig. 1a). Similar features were observed in the same regions for different samples of crystalline GB1, measured at different conditions, suggesting that they may not be due to random error. At the same time, in spite of extensive control measurements, we were not able to identify the origin of such features or reproduce them in simulations.

To quantify the microsecond exchange processes in crystalline GB1 in diamagnetic and paramagnetic samples, we fitted the data for residues showing clear dispersion at two magnetic fields (14.1 and 16.4 T) to the two-site exchange Bloch-McConnell formalism (eq. 1, see Methods)[37,38]. All residues were fitted individually and in groups. Residues that were close in space displayed very similar exchange rates when fitted individually (see Supplementary Table S2) and were consequently clustered into groups to fit them simultaneously. This is permissible, assuming that the clustered residues undergo a common motion, or, more specifically, share a common exchange rate, k_{ex}, and have the same populations of exchanging states, p_A & p_B, but with residue specific chemical shift differences between the states, $\Delta\delta$. Because the populations and chemical shift differences are highly correlated and difficult to extract from the fits, φ_{ex}, the product between p_A, p_B and $\Delta\delta^2$ is used as a single fit parameter.

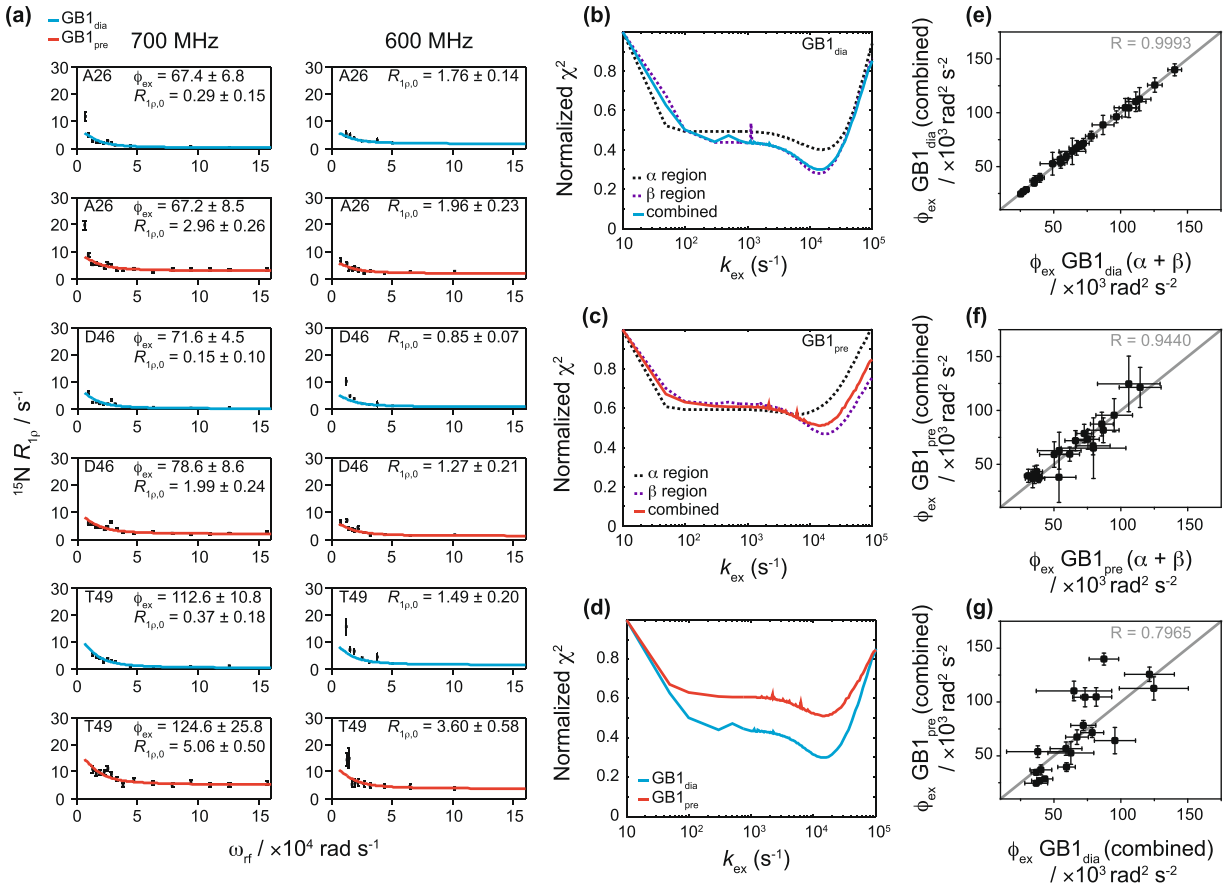

Figure 1. ^{15}N $R_{1\rho}$ relaxation dispersion for crystalline GB1. (**a**) Example fits based on the data from the sample without paramagnetic dopant ($GB1_{dia}$) (blue lines, $k_{ex} = 14 \pm 0.5 \times 10^3\,s^{-1}$) and the sample with paramagnetic dopant ($GB1_{pre}$) (red lines, $k_{ex} = 15 \pm 2 \times 10^3\,s^{-1}$) obtained from measurements at 600 MHz (14.1 T) and 700 MHz (16.4 T) and a sample temperature of 300 ± 2 K. For simplicity the units for the residue specific φ_{ex} and $R_{1\rho,0}$ are omitted in the graphs and are $\times 10^3$ rad^2 s^{-2} and s^{-1}, respectively. (**b**–**d**) Agreement between experimental and fitted data represented by plots between fixed exchange coefficients, k_{ex}, and the corresponding normalized χ^2 values from joint fitting of relaxation dispersion curves for different groupings of residues in $GB1_{dia}$ (**b**) and $GB1_{pre}$ (**c**), as well as a comparison of normalised χ^2 values from global fits in $GB1_{dia}$ and $GB1_{pre}$ (**d**). The fits obtained from the different groupings are indicated with dotted black lines for the α-helix region, dotted purple lines for the β–sheet region and solid lines for all residues together (blue for $GB1_{dia}$ and red for $GB1_{pre}$). (**e**, **f**) Correlation plots for φ_{ex} values based on fits of all residues together and the α-helix and β-sheet regions separately for $GB1_{dia}$ (**e**) and $GB1_{pre}$ (**f**). (**g**) Correlation plot for φ_{ex} values based on fits of all residues together between $GB1_{dia}$ and $GB1_{pre}$. The correlation coefficient (R) is indicated in grey in each correlation plot.

We fitted residues in the α-helix and β-sheet regions separately and together (see Fig. 1a for representative relaxation dispersion curves for $GB1_{dia}$ and $GB1_{pre}$ and Supplementary Tables S2–9 and Figs S9–10 for results from all residues). The obtained k_{ex} for $GB1_{dia}$ were very similar between the different group fits: $14 \pm 0.5 \times 10^3\,s^{-1}$ for all residues together, $14 \pm 1 \times 10^3\,s^{-1}$ for the β-sheet region and $16 \pm 1 \times 10^3\,s^{-1}$ for the α-helix region. For $GB1_{pre}$ there were, however, some differences between the group fits: $15 \pm 2 \times 10^3\,s^{-1}$ for all residues together, $14 \pm 2 \times 10^3$ for the β-sheet region and $6 \pm 2 \times 10^3\,s^{-1}$ for the α-helix region. To investigate the difference in k_{ex} rates between the α-helix and β-sheet regions in $GB1_{pre}$, we plotted the χ^2 values (see Eq. 8 in the Methods part) as a function of varied k_{ex} (Fig. 1b, c). For $GB1_{dia}$ the lowest χ^2 values (equivalent to the best fits) are obtained for the same k_{ex} values regardless of whether the α helix and β sheet regions are fitted individually or together. However, if the α region of $GB1_{pre}$ is fitted alone (Fig. 1c, dotted black line), the curve has a shallow minimum suggesting k_{ex} is not well restrained by the data in this case. Correlation plots between the obtained φ_{ex} values from fits of the α helix and β sheet regions separately and all residues together show excellent agreement with correlation coefficients (R values) of 0.9993 and 0.9440 for $GB1_{dia}$ (Fig. 1e) and $GB1_{pre}$ (Fig. 1f), respectively. To further evaluate the different models, we calculated Bayesian Information Criterion values (BIC, see Methods, Eq. 9). The lowest BIC values were yielded by a global group fit including all residues showing dispersion (see Supplementary Table S10), suggesting that, statistically, this is the best model. A comparison between the global fits for all residues exhibiting dispersion in $GB1_{dia}$ and $GB1_{pre}$ (Fig. 1d) show clear narrow minima in the same regions of k_{ex}. Overall, the parameters of the exchange processes obtained from $GB1_{pre}$ agree reasonably well with the data for $GB1_{dia}$ with

excellent agreements between the k_{ex} values ($14 \pm 0.5 \times 10^3\,s^{-1}$ for $GB1_{dia}$ and $15 \pm 2 \times 10^3\,s^{-1}$ for $GB1_{pre}$) and a good correlation between φ_{ex} values for most residues (Fig. 1g). This confirms that although the paramagnetic agent affects $R_{1\rho}$ relaxation rates, it does not affect the exchange contribution.

Encouraged by the reasonable agreement for the microsecond exchange between crystalline $GB1_{dia}$ and $GB1_{pre}$, we applied the accelerated relaxation dispersion approach to a more challenging system, GB1 in a >300 kDa complex with IgG. Performing ^{15}N $R_{1\rho}$ relaxation dispersion on a diamagnetic sample of the complex would require unpractically long experimental times with each $R_{1\rho}$ measurement requiring ~3–5 days to obtain SNRs sufficient for quantitative analysis[3,39]. Experimental times on the order of 1–2 months would be necessary for full relaxation dispersion measurement. Even if such long times could be dedicated to a single experiment, maintaining sufficient experimental stability over the duration is very challenging. The addition of Gd(DTPA-BMA) yielded an increase in SNR per time unit of about 5 in the complex (based on 2D HN correlation spectra, see Supplementary Table S1). This allowed us to perform these experiments in 5 days on an 850 MHz spectrometer (20 T) on a sample with 5 mM Gd(DTPA-BMA) and in 10 days on a 700 MHz spectrometer (16.4 T) on a sample with 2 mM Gd(DTPA-BMA), using 10 different spin-lock field strengths at each B_0 field (experimental durations are shown in Supplementary Table S10 and examples of $R_{1\rho}$ fits are shown in Supplementary Fig. S.11).

In our experiments, many of the residues that exhibit relaxation dispersion in GB1 crystals also do so in the complex with IgG. In the β-sheet region, dispersion was observed for the same residues with the exception of residue 38, which is located in the loop region between the α-helix and the β3 strand. Gly38 showed clear dispersion in the GB1:IgG complex but not in crystalline GB1 (see Supplementary Figs S2–9; note that data for some residues that show μs exchange in crystalline GB1 could not be obtained due to either severe overlap or insufficient signal to noise in the GB1:IgG complex, including several residues in the α helix). In addition, the dispersion at the C-terminal end of β4 in the complex was less clear compared to crystalline GB1, especially at the lower magnetic field. A possible explanation for this discrepancy could be the presence of additional intermolecular interactions in the complex that either slow down conformational exchange or restrict its amplitude. We have recently proposed the existence of such an additional interaction interface in the complex with full length IgG, based on chemical shift perturbations[4] and solvent PREs[39]. Interestingly, in contrast to crystalline GB1, in the complex none of the residues in the α-helix showed clear dispersion at either B_0 field (see Supplementary Fig. S12 for a summary of which residues show dispersion), indicating that the motion we observed for the α helix in the crystalline sample is either too slow to detect in experiments with the lowest spin lock frequency of ~2 kHz or is not present at all in the complex.

Since all residues showing dispersion in the GB1:IgG complex were located in the β-sheet region, we considered them as being involved in the same motion and fitted them together to obtain a single value for k_{ex} ($13 \pm 3 \times 10^3\,s^{-1}$; see Fig. 2). The best fit parameters for GB1:IgG are listed in Supplementary Tables S12,13 (the fits for individual residues are also included for completeness). To investigate if there were separate motions of the individual binding sites to the Fab and Fc fragments of IgG, we grouped the residues close to each binding site and fitted each group separately. This yielded essentially identical results to fits of all residues combined (see Supplementary Tables S14,15 and Fig. S13).

Overall, we observed relaxation dispersion in similar regions as in earlier, qualitative measurements of GB1 in complex with IgG[3]. However, several false positives from this approximate method, together with need of quantification, highlight the importance of measuring full relaxation dispersion curves.

Discussion

Somewhat unexpectedly, the results of ^{15}N $R_{1\rho}$ relaxation dispersion experiments suggest that, in crystalline GB1 and in GB1 in the complex with IgG, slow conformational exchange occurs for nearly identical sets of residues in the β-sheet. Moreover, the process is characterized by similar microsecond exchange rates. A direct comparison of these results to an isolated molecule of GB1 in solution is not possible because, to the best of our knowledge, relaxation dispersion for the same GB1 construct has not been reported in the literature. The most closely related protein for which such solution NMR data are available is GB3 that has the same fold as GB1 but differs by 6 residues[40]. Such differences could potentially lead to modification of dynamic behavior of the protein but comparison of patterns of motions could still be informative. No microsecond exchange was detected at room temperature for GB3[40]. Low microsecond exchange was detected in loop 1 of GB3 only under supercooled conditions (residues 9–13, which are the same between GB1 and GB3)[40]. Extrapolated to room temperature, this exchange process would occur on the order of hundreds of nanoseconds, which is too fast to induce relaxation dispersion in the here considered regime. Indeed, in the crystalline sample of GB1, we do not observe relaxation dispersion for any residues in loop 1, with the exception of Leu12. This is consistent with extended model free analysis of ^{15}N and $^{13}C'$ relaxation rates in crystalline GB1 at room temperature, which places the slow backbone motions in loop 1 in the range of hundreds of nanoseconds[41]. Thus, the available solution NMR relaxation dispersion data do not help to shed light on the potential origins of the microsecond motions detected in the solid state. The most likely explanation for the motions observed in the solid-state is that intermolecular interactions lead to increased energy barriers between subsets of interconverting conformations. Higher energy barriers would cause the concerned motions to be slower than in an isolated molecule in solution. The influence of intermolecular interactions on slow motions has been observed previously: in ubiquitin, the main slow conformational exchange process is present in solution and in crystals but appears much slower in the latter[13,15,42]. In the case of GB1, different intermolecular interactions seem to lead to a slowing down of a subset of motions that are too fast to be picked up by relaxation dispersion in solution. A combination of RDC measurements and molecular dynamics simulations of GB3 and GB1 in solution has suggested a presence of slow correlated motions across the β-sheet[43–45]. These motions are the most likely to be slowed down by intermolecular interactions to yield patterns observable through relaxation dispersion in the solid state. The characteristics of the motions in the β-sheet region in crystalline GB1 and the GB1:IgG complex are the most similar near the β2 strand. There, the pattern of intermolecular

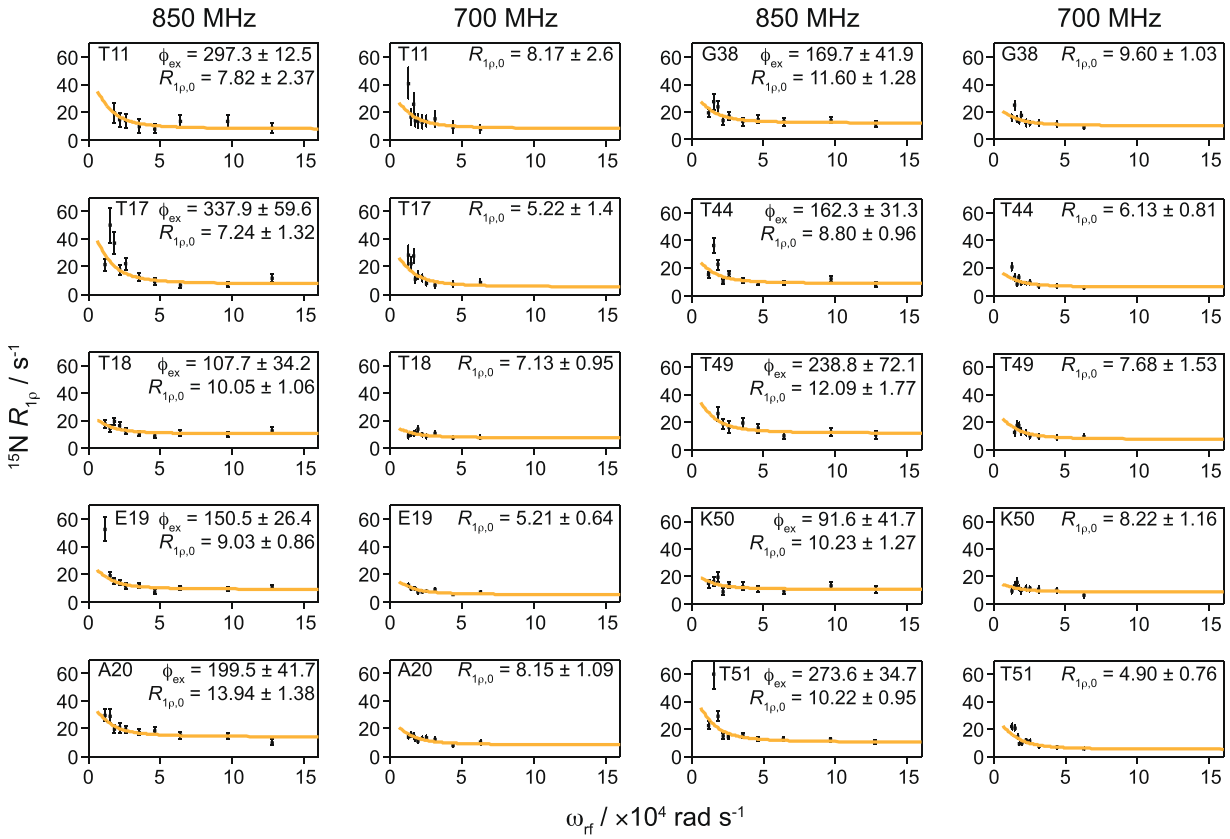

Figure 2. ^{15}N $R_{1\rho}$ relaxation dispersion profiles for GB1 in complex with IgG. Experiments were acquired at 700 MHz (16.4 T) with 2 mM Gd(DTPA-BMA) and 850 MHz (20 T) with 5 mM Gd(DTPA-BMA), and a sample temperature of 300 ± 2 K. Best fit curves to a two-site exchange model assuming a common motion are shown as orange lines ($k_{ex} = 13 \pm 3 \times 10^3\ s^{-1}$). Residue specific φ_{ex} ($\times 10^3$ rad^2 s^{-2}) and $R_{1\rho,0}$ (s^{-1}) are indicated in each plot.

hydrogen bonds between two GB1 molecules in the crystal is very similar to the hydrogen bonds present between GB1 and the Fab fragment of IgG in the complex. The differences in the pattern of microsecond motions increase towards the β3 strand, where a set of intermolecular hydrogen bonds is present between GB1 molecules in the crystal but a different interaction interface is formed with the Fc fragment in the complex. The microsecond exchange observed for residues in the α-helix in crystalline GB1 and the apparent absence of similar motions in the complex could also be linked to different intermolecular interactions. In the crystals, the helix is packed more densely than in the complex with IgG[4,39,46,47], which likely leads to increased energy barriers for helix motions in the crystal. Finally, we observe differences between φ_{ex} values in crystalline GB1 and GB1 in complex with IgG. These parameters are linked to the populations of the exchanging states and the chemical shift difference between the states. In crystalline GB1 the φ_{ex} values are between 25–140 $\times 10^3$ rad^2 s^{-2}, with the lower values in the α-helix and higher values in β strands and loop regions. The φ_{ex} values for GB1 in complex with IgG are significantly larger, 90–300 $\times 10^3$ rad^2 s^{-2}, suggesting that either the population of the minor state or the chemical shift differences between the states (or both) are larger in the complex than in the crystals.

In general, the presence of μs motions should induce spinning frequency dependence of $R_{1\rho}$[14]. Whereas previously we observed a very strong spinning frequency dependence of $R_{1\rho}$ rates in the GB1:IgG complex, most residues in crystalline GB1 showed, within the experimental error, weak or no spinning frequency dependence (see also Supplementary Fig. S16)[3]. In order to see how we can reconcile these data, we modelled ^{15}N $R_{1\rho}$ rates for residues showing dispersion in the β-sheet in crystalline GB1 using the simple model free formalism. Fitting of the data for each residue (at 39, 50 and 56 kHz MAS speeds at 14.1 T and 50 kHz and 60 kHz at 16.4 T, sample temperature ~300 K, data from ref.[3]) with the time scale fixed to the inverse of the average of k_{ex} for $GB1_{dia}$ and $GB1_{pre}$ ($1/(15 \times 10^3\ s^{-1}) = 67$ μs), the best-fit order parameters for the slow motions are between 0.998–0.983. To obtain such high order parameters, either the amplitude of the motion needs to be very small when the population of the minor state is relatively large or the amplitude of motion can be larger when the population of the minor state is small[48]. For example, in a two-site jump model with unequal populations, those order parameters correspond to a jump angle between 7–20° for a minor population of 5% and a jump angle of 3–9° for equal populations of the two states (see Supplementary Fig. S14).

The ^{15}N $R_{1\rho}$ relaxation dispersion data suggest that in both samples, crystalline GB1 and GB1 in the complex with IgG, microsecond motions are present and span the β-sheet at 300 K. Whereas at 300 K the data do not suggest additional microsecond motions in crystalline GB1 beyond the ones detected through relaxation dispersion, the spinning frequency dependency of ^{15}N $R_{1\rho}$ for GB1 in the complex is consistent with the presence of

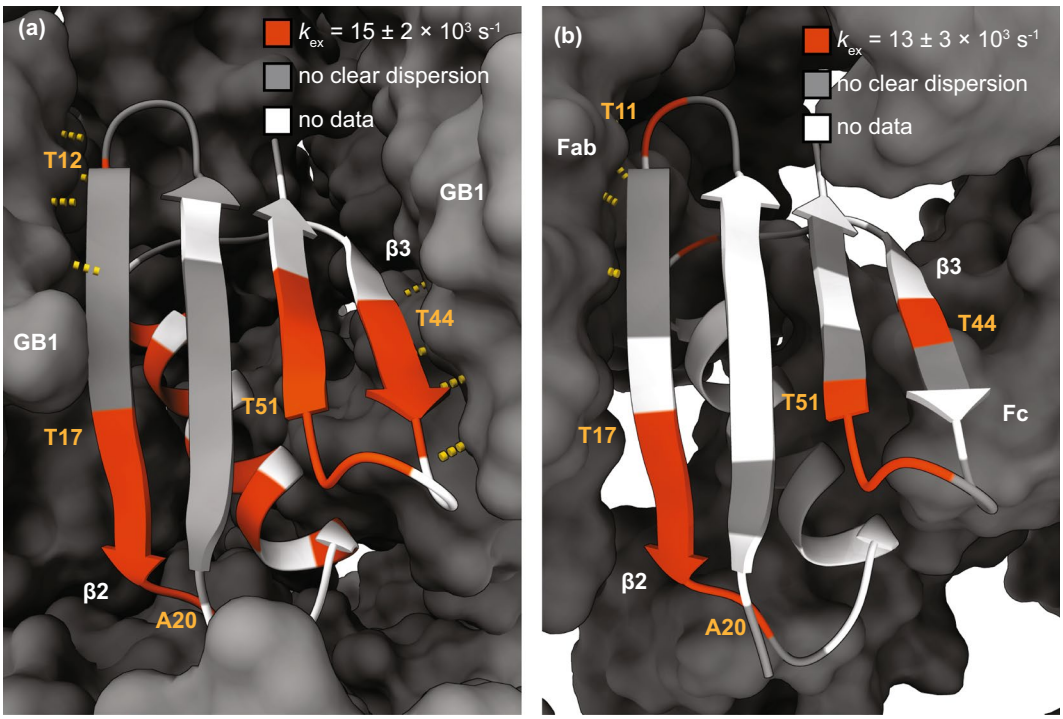

Figure 3. Microsecond exchange in crystalline GB1 (**a**) and GB1 in a complex with IgG (**b**). Residues showing relaxation dispersion are shown in orange. Exchange rates for group fits of the regions are given above the figures. White indicates residues for which data are missing. Grey represents residues with no clear relaxation dispersion. Yellow dashed lines represent hydrogen bonds.

an additional small amplitude overall motion in the microsecond range. For many sites such an overall motion would not induce significant isotropic chemical shift modulation (since no local conformation change is involved) and thus would not lead to relaxation dispersion in the regime considered here[3]. On a side note, the bulk ^{15}N NERRD data obtained on crystalline GB1 at a lower spinning frequency (20 kHz) and lower sample temperature (293 K) was previously attributed to ultralow amplitude overall rocking of the molecule[49]. However, under conditions employed in ref.[3] (40–60 kHz MAS and 300 K) such a motion would result in negligible spinning frequency dependence of ^{15}N $R_{1\rho}$ (see also Supplementary Fig. S16 where these data are replotted).

In summary, we have shown that the addition of a paramagnetic agent to hydrated solid state NMR samples permits relaxation dispersion measurements in systems such as large protein complexes, where otherwise low sensitivity prevents data collection in a realistic time frame. In our sample, a >300 kDa precipitated complex of GB1:IgG, the increase in SNR per time unit was on the order of 5, which allowed us to obtain quantitative measurements in 1–2 weeks on samples containing a few dozens of micrograms of labelled GB1 in the complex. Our experiments revealed the presence of similar microsecond motions in the β-sheet in both crystalline GB1 and in the GB1:IgG complex. In contrast, microsecond motions in the α-helix observed in crystalline GB1 appear to be absent in GB1 in the complex with IgG. Overall, the microsecond motions detected using relaxation dispersion do not account for the large differences in ^{15}N $R_{1\rho}$ measured in the two different assemblies[3], supporting the idea of an additional small amplitude overall motion being present in the GB1:IgG complex. Overall, these results highlight the importance of direct measurements in complex assemblies to complement studies of their isolated components. Such experiments aid our understanding of the dynamics in interacting systems on a molecular level. Our approach will enable similar measurements on other complex systems, which are beyond the reach of current approaches.

Methods

Sample preparation. Isotope labelled [U-^{2}H,^{13}C,^{15}N]GB1 2Q6I was expressed as described before[39]. In brief, BL21(DE3) cells transformed with pGEV2[50] were grown in LB until they reached an OD600 > 1.0. The cells were washed once with PBS before resuspension in M9 with D_2O, deuterated [U-^{13}C]glucose and $^{15}NH_4Cl$ and expression was induced with 0.5 mM IPTG after 1 h incubation at 37 °C. The protein was expressed for 4 h at 37 °C before the cells were harvested by centrifugation (4000 × G for 20 min at 16 °C) and lysed by sonication (50 mM potassium phosphate; 200 mM NaCl; 1 mg/ml lysozyme; pH 7.0). After heat treatment at 75 °C for 10 min, the lysate was cleared by centrifugation (12000 × G for 50 min). GB1 was precipitated over night with 80% ammonium sulfate and collected by centrifugation (15000 × G for 50 min). The pellet was resuspended in buffer (50 mM potassium phosphate; 200 mM NaCl; pH 7.0), and purified on a 16/600 Sephadex pg75 (GE Healthcare) gel filtration column. Fractions containing GB1 were collected, desalted, freeze-dried and stored at −20 °C.

Freeze-dried [U-^{2}H,^{13}C,^{15}N]GB1 was dissolved in buffer (50 mM sodium phosphate buffer; pH 5.5) to obtain a protein concentration of 10 mg/ml and crystallized with the aid of 2:1 2-methyl-2,4-pentanediol (MPD):Isopropanol[51]. The GB1:IgG complex was formed by mixing GB1 and IgG (Sigma – Aldrich, lyophilized, human serum) solutions in a 2:1 molar ratio[4]. Crystalline GB1 and precipitated GB1:IgG complex were packed into NMR rotors using the following procedure: The crystals/precipitate were collected by centrifugation (1 min at 20 000 × G using a bench top centrifuge), and resuspended in a small volume of the supernatant containing 2% DSS and Gd(DTPA–BMA) at the desired concentration. The samples were transferred into 200 µl pipette tips, which were then attached to the rotors, put into 1.5 ml Eppendorf tubes and centrifuged (20 000 × G) in 1–4 minutes intervals until the rotors were full. The rotor caps were sealed with a silicone-based glue to prevent leakage.

Solid state NMR. Solid state NMR spectra were recorded at 600 MHz Bruker Avance II+, 700 MHz Bruker Avance III HD and 850 MHz Bruker Avance III spectrometers, using Bruker 1.3 mm triple resonance probes at 60 kHz magic angle spinning. A Bruker BCU-X cooling unit was used to regulate the internal sample temperature to 27 ± 2 °C (measured from the chemical shift of water with respect to DSS). For experiments recorded at 700 MHz ^{1}H Larmor frequency with the GB1:IgG complex, 10% D_2O was added to the sample buffer before packing the rotors and deuterium locking was used in the same way as in solution NMR. ^{15}N-^{1}H 2D correlation spectra were recorded using a proton-detected heteronuclear correlation sequence. Double quantum cross-polarization (CP) contact times were between 0.5–1.5 ms and individually optimized for each sample. Recycle delays between 0.2–2 s were used depending on the amount of paramagnetic agent and magnetic field (see Supplementary Table S11). The optimal recycle delay for each sample was selected by comparing signal to noise ratios in 1D planes recorded with the same sequence as the 2D ^{1}H-^{15}N correlation experiments. $R_{1\rho}$ relaxation dispersion experiments were recorded as several pseudo 3Ds with the varying spin-lock lengths as the 3rd dimension and with different spin-lock power in each 3D experiment or a pseudo 4D (GB1:IgG complex at 850 MHz ^{1}H Larmor frequency) with the varying spin-lock power as the 4th dimension. In all solid-state experiments, hard pulses were applied at nutation frequencies of 100 kHz for ^{1}H and 83.3 kHz for ^{15}N. 10 kHz WALTZ-16 decoupling was applied on protons during ^{15}N evolution, and on the ^{15}N channel during direct ^{1}H acquisition, while quadrature detection was achieved using the States-TPPI method. Suppression of the water signal was achieved by saturation with 50–200 ms of slpTPPM ^{1}H decoupling applied at an amplitude of ¼ of the MAS frequency[52] or 100–140 ms MISSISSIPPI[53] at an amplitude of ½ the MAS frequency on resonance with the water signal. $R_{1\rho}$ relaxation curves were sampled using 7–10 points for all experiments. 1–25 kHz nutation frequencies, measured by nutation experiments, were used for the spin-lock fields in the $R_{1\rho}$ experiments (see SI table 13 for number of points used and total duration of the experiments). Residues which are far away from the center of the spectra in the ^{15}N dimension and not covered by the spin-lock pulse were removed. These included; $GB1_{dia}$ at 700 MHz ^{1}H Larmor frequency and 1.1 kHz spin-lock frequency (6, 8, 9, 11, 12, 14, 19, 20, 38, 40, 41, 44, 46, 49, 52, 56), $GB1_{dia}$ at 700 MHz ^{1}H Larmor frequency and 1.5 kHz spin-lock frequency (11, 14, 40, 49, 52, 56), $GB1_{pre}$ at 700 MHz ^{1}H Larmor frequency and 1 kHz spin-lock frequency (2, 6, 8, 9, 11, 12, 14, 19, 40, 44, 46, 49, 52, 56) $GB1_{pre}$ at 700 MHz ^{1}H Larmor frequency and 1.5 kHz spin-lock frequency (11, 14, 40, 49, 52, 56), $GB1_{pre}$ at 600 MHz ^{1}H Larmor frequency and 1.2 kHz spin-lock frequency (11, 12, 14, 40, 49, 52, 56), GB1 in complex with IgG at 850 MHz ^{1}H Larmor frequency and 1.85 kHz spin-lock frequency (11, 40, 49, 52, 56), GB1 in complex with IgG at 850 MHz ^{1}H Larmor frequency and 2.45 kHz spin-lock frequency (11, 49), GB1 in complex with IgG at 700 MHz ^{1}H Larmor frequency and 2 kHz spin-lock frequency (49, 56). All spectra were processed using TopSpin 3.2. GB1 resonances in the complex with IgG were previously assigned on the basis of 3D H(H)NH, CONH, CO(CA)NH and CANH experiments[4]. Peak integrals were calculated in TopSpin 3.2. OriginPro 2016 and MatLab R2014a were used to analyze the relaxation data.

Data fitting. Peak integrals from TopSpin were exported to MatLab where a mono-exponential function was used with the fminsearchbnd function to fit the relaxation data. Average values calculated from integral regions containing only noise were used as input errors. Fit errors were calculated by Monte Carlo error estimations. A random number between 0 and 1 was multiplied with the integral error and added to the recalculated integrals. The fitting was then repeated 2000 times with a new random number between 0 and 1 generated each time. Two times the standard deviations of the $R_{1\rho}$ values received from the fits for each residue were used as errors.

Exchange coefficients (k_{ex}), populations of the minor state and major sites ($p_A p_B$), and difference in chemical shifts between the two states ($\Delta\delta$) were obtained by fitting the $R_{1\rho}$ values obtained at two different B_0 fields simultaneously to a Bloch-McConnell two-site exchange Eq. (1) derived as described in[37,38]. Since the populations and the chemical shift differences are highly correlated, the product of the two, φ_{ex}, was extracted from the fits instead.

$$R_{1\rho} = R_{1\rho,0} + \frac{p_A p_B \Delta\delta^2 k_{ex}}{\omega_1^2 + k_{ex}^2} \quad (1)$$

where $R_{1\rho,0}$ is the plateau value for $R_{1\rho}$ and ω_1 is the ^{15}N spin-lock field strength. For the higher B_0 field used in the fits the ratio between the fields squared was multiplied with the fraction in the equation to account for the differences in field strengths. Errors were calculated using Monte Carlo error estimation in the same way as for $R_{1\rho}$ exponential fits but with 250 repeats of the fitting. In these fits, on resonance $R_{1\rho}$ rates were used, and were calculated from the measured rates ($R_{1\rho,obs}$) by Eq. 2:

$$R_{1\rho} = \frac{R_{1\rho,obs} - \cos^2\theta R_1}{\sin^2\theta} \quad (2)$$

where the R_1 rates used are published elsewhere[3,39] and the angle θ was calculated from Eq. 3 with Ω as the offset for each peak.

$$\theta = \tan^{-1}\frac{\omega_1}{\Omega} \tag{3}$$

For modelling of spinning frequency dependent ^{15}N $R_{1\rho}$, both, dipolar NH ($r_{NH} = 1.02$ Å) and ^{15}N chemical shift anisotropy (CSA (assuming axially symmetric CSA tensor collinear with the NH vector; $\Delta\sigma = \sigma_{\parallel} - \sigma_{\perp} = -170$ ppm, $\eta = 0$) contributions, were considered.

The dipolar contribution was expressed as[3,14]

$$\begin{aligned} R_{1\rho,NH} \;=\; & \frac{1}{20}\left(\frac{\mu_0}{4\pi}\frac{\hbar\gamma_H\gamma_N}{r_{NH}^3}\right)^2\left(\frac{2}{3}J\left(\omega_1 + 2\omega_r\right) + \frac{2}{3}J\left(\omega_1 - 2\omega_r\right) + \frac{4}{3}J\left(\omega_1 + \omega_r\right)\right. \\ & + \frac{4}{3}J\left(\omega_1 - \omega_r\right) + 3J\left(\omega_N\right) \\ & \left. + J\left(\omega_H - \omega_N\right) + 6J\left(\omega_H\right) + 6J\left(\omega_H + \omega_N\right)\right) \end{aligned} \tag{4}$$

and CSA contribution

$$R_{1\rho,NCSA} = \frac{1}{45}(\sigma_{\parallel} - \sigma_{\perp})^2\left(\frac{2}{3}J\left(\omega_1 + 2\omega_r\right) + \frac{2}{3}J\left(\omega_1 - 2\omega_r\right) + \frac{4}{3}J\left(\omega_1 + \omega_r\right) + \frac{4}{3}J\left(\omega_1 - \omega_r\right) + 3J\left(\omega_N\right)\right) \tag{5}$$

where ω_r is the spinning frequency, ω_1 is the spin lock nutation frequency, and ω_N, ω_H the nitrogen and proton Larmor frequencies, respectively.

The expression for the order parameter of the two-site jump model was[54]

$$S^2 = \sum_{i,j}\frac{p_i p_j}{2}(3\cos^2\theta - 1) \tag{6}$$

where p_i, p_j are the populations of the two states and θ is the jump angle.

The simple model free spectral density was defined as

$$J(\omega) = (1 - S^2)\frac{\tau}{1 + (\omega\tau)^2} \tag{7}$$

The fitting of the data was done by minimization of the χ^2 target function:

$$\chi^2 = \sum\frac{\left(X_{i,calc} - X_{i,\exp}\right)^2}{\sigma_{i,\exp}^2} \tag{8}$$

where χ_i are the data sets and σ_i the corresponding error.

In fits where data from two magnetic fields were combined the minimization of the χ^2 target functions for both magnetic fields was performed simultaneously. To adjust for the different number of spin-lock fields used for crystalline GB1 at different magnetic fields, a weighting factor was used so that data from each magnetic field is contributing equally to the final χ^2 value. The weighting factor was determined by comparing the minimum χ^2 value obtained by fitting data from each magnetic field separately (see Supplementary Fig. S15).

To compare how different models performed, the Bayesian Information Criterion (BIC) was calculated for each model as:

$$BIC = \chi^2 + k\ln(n) \tag{9}$$

where k is the number of fit parameters and n the number of data points (see Supplementary Table S10 for comparisons between different models).

Data Availability

Raw NMR data is available on WRAP at the link: http://wrap.warwick.ac.uk/117521/.

References

1. Palmer, A. G. & Massi, F. Characterization of the Dynamics of Biomacromolecules Using Rotating-Frame Spin Relaxation NMR Spectroscopy. *Chem. Rev.* **106**, 1700–1719 (2006).
2. Schanda, P. & Ernst, M. Studying dynamics by magic-angle spinning solid-state NMR spectroscopy: Principles and applications to biomolecules. *Prog. Nucl. Magn. Reson. Spectrosc.* **96**, 1–46 (2016).
3. Lamley, J. M., Öster, C., Stevens, R. A. & Lewandowski, J. R. Intermolecular Interactions and Protein Dynamics by Solid-State NMR Spectroscopy. *Angew. Chemie Int. Ed.* **54**, 15374–15378 (2015).
4. Lamley, J. M. *et al.* Solid-State NMR of a Protein in a Precipitated Complex with a Full-Length Antibody. *J. Am. Chem. Soc.* **136**, 16800–16806 (2014).
5. Struppe, J. *et al.* Expanding the horizons for structural analysis of fully protonated protein assemblies by NMR spectroscopy at MAS frequencies above 100 kHz. *Solid State Nucl. Magn. Reson.*, https://doi.org/10.1016/j.ssnmr.2017.07.001 (2017).
6. Barbet-Massin, E., Huang, C.-T., Daebel, V., Hsu, S.-T. D. & Reif, B. Site-Specific Solid-State NMR Studies of "Trigger Factor" in Complex with the Large Ribosomal Subunit 50S. *Angew. Chemie Int. Ed.* **54**, 4367–4369 (2015).

7. Mainz, A. *et al*. NMR Spectroscopy of Soluble Protein Complexes at One Mega-Dalton and Beyond. *Angew. Chemie Int. Ed.* **52**, 8746–8751 (2013).
8. Gardiennet, C. *et al*. A Sedimented Sample of a 59 kDa Dodecameric Helicase Yields High-Resolution Solid-State NMR Spectra. *Angew. Chemie Int. Ed.* **51**, 7855–7858 (2012).
9. Lu, M. *et al*. Dynamic allostery governs cyclophilin A–HIV capsid interplay. *Proc. Natl. Acad. Sci.* **112**, 14617–14622 (2015).
10. Dannatt, H. R. W. *et al*. Weak and Transient Protein Interactions Determined by Solid-State NMR. *Angew. Chemie Int. Ed.* **55**, 6638–6641 (2016).
11. Demers, J.-P. *et al*. High-resolution structure of the Shigella type-III secretion needle by solid-state NMR and cryo-electron microscopy. *Nat. Commun.* **5**, 4976 (2014).
12. Marion, D., Gauto, D. F., Ayala, I., Giandoreggio-Barranco, K. & Schanda, P. Microsecond Protein Dynamics from Combined Bloch-McConnell and Near-Rotary-Resonance R 1 p Relaxation-Dispersion MAS NMR. *ChemPhysChem* **20**, 276–284 (2019).
13. Kurauskas, V. *et al*. Slow conformational exchange and overall rocking motion in ubiquitin protein crystals. *Nat. Commun.* **8**, 145 (2017).
14. Kurbanov, R., Zinkevich, T. & Krushelnitsky, A. The nuclear magnetic resonance relaxation data analysis in solids: general R1/R1(ρ) equations and the model-free approach. *J. Chem. Phys.* **135**, 184104 (2011).
15. Ma, P. *et al*. Probing transient conformational states of proteins by solid-state R 1ρ relaxation-dispersion NMR spectroscopy. *Angew. Chemie - Int. Ed.* **53**, 4312–4317 (2014).
16. Parthasarathy, S., Nishiyama, Y. & Ishii, Y. Sensitivity and Resolution Enhanced Solid-State NMR for Paramagnetic Systems and Biomolecules under Very Fast Magic Angle Spinning. *Acc. Chem. Res.* **46**, 2127–2135 (2013).
17. Ullrich, S. J., Hölper, S. & Glaubitz, C. Paramagnetic doping of a 7TM membrane protein in lipid bilayers by Gd3+-complexes for solid-state NMR spectroscopy. *J. Biomol. NMR* **58**, 27–35 (2014).
18. Nadaud, P. S., Helmus, J. J., Kall, S. L. & Jaroniec, C. P. Paramagnetic Ions Enable Tuning of Nuclear Relaxation Rates and Provide Long-Range Structural Restraints in Solid-State NMR of Proteins. *J. Am. Chem. Soc.* **131**, 8108–8120 (2009).
19. Nadaud, P. S., Helmus, J. J., Höfer, N. & Jaroniec, C. P. Long-Range Structural Restraints in Spin-Labeled Proteins Probed by Solid-State Nuclear Magnetic Resonance Spectroscopy. *J. Am. Chem. Soc.* **129**, 7502–7503 (2007).
20. Pintacuda, G. *et al*. Solid-State NMR Spectroscopy of a Paramagnetic Protein: Assignment and Study of Human Dimeric Oxidized CuII–ZnII Superoxide Dismutase (SOD). *Angew. Chemie Int. Ed.* **46**, 1079–1082 (2007).
21. Jaroniec, C. P. Solid-state nuclear magnetic resonance structural studies of proteins using paramagnetic probes. *Solid State Nucl. Magn. Reson.* **43–44**, 1–13 (2012).
22. Wickramasinghe, N. P. *et al*. Nanomole-scale protein solid-state NMR by breaking intrinsic 1H T1 boundaries. *Nat. Methods* **6**, 215–218 (2009).
23. Jaroniec, C. P. Structural studies of proteins by paramagnetic solid-state NMR spectroscopy. *J. Magn. Reson.* **253**, 50–59 (2015).
24. Knight, M. J. *et al*. Structure and backbone dynamics of a microcrystalline metalloprotein by solid-state NMR. *Proc. Natl. Acad. Sci.* **109**, 11095–11100 (2012).
25. Wickramasinghe, N. P., Kotecha, M., Samoson, A., Past, J. & Ishii, Y. Sensitivity enhancement in 13C solid-state NMR of protein microcrystals by use of paramagnetic metal ions for optimizing 1H T1 relaxation. *J. Magn. Reson.* **184**, 350–356 (2007).
26. Nadaud, P. S., Helmus, J. J., Sengupta, I. & Jaroniec, C. P. Rapid Acquisition of Multidimensional Solid-State NMR Spectra of Proteins Facilitated by Covalently Bound Paramagnetic Tags. *J. Am. Chem. Soc.* **132**, 9561–9563 (2010).
27. Ward, M. E. *et al*. High-resolution paramagnetically enhanced solid-state NMR spectroscopy of membrane proteins at fast magic angle spinning. *J. Biomol. NMR* **58**, 37–47 (2014).
28. Balayssac, S., Bertini, I., Bhaumik, A., Lelli, M. & Luchinat, C. Paramagnetic shifts in solid-state NMR of proteins to elicit structural information. *Proc. Natl. Acad. Sci.* **105**, 17284–17289 (2008).
29. Linser, R., Fink, U. & Reif, B. Probing Surface Accessibility of Proteins Using Paramagnetic Relaxation in Solid-State NMR Spectroscopy. *J. Am. Chem. Soc.* **131**, 13703–13708 (2009).
30. Sengupta, I., Nadaud, P. S. & Jaroniec, C. P. Protein Structure Determination with Paramagnetic Solid-State NMR Spectroscopy. *Acc. Chem. Res.* **46**, 2117–2126 (2013).
31. Rovó, P. & Linser, R. Microsecond Timescale Protein Dynamics: a Combined Solid-State NMR Approach. *ChemPhysChem* **19**, 34–39 (2018).
32. Rovó, P. *et al*. Mechanistic Insights into Microsecond Time-Scale Motion of Solid Proteins Using Complementary 15 N and 1 H Relaxation Dispersion Techniques. *J. Am. Chem. Soc.* **141**, 858–869 (2019).
33. Cai, S., Seu, C., Kovacs, Z., Sherry, A. D. & Chen, Y. Sensitivity Enhancement of Multidimensional NMR Experiments by Paramagnetic Relaxation Effects. *J. Am. Chem. Soc.* **128**, 13474–13478 (2006).
34. Hocking, H. G., Zangger, K. & Madl, T. Studying the Structure and Dynamics of Biomolecules by Using Soluble Paramagnetic Probes. *ChemPhysChem* **14**, 3082–3094 (2013).
35. Lewandowski, J. R., Sass, H. J. J., Grzesiek, S., Blackledge, M. & Emsley, L. Site-specific measurement of slow motions in proteins. *J. Am. Chem. Soc.* **133**, 16762–5 (2011).
36. Lewandowski, J. R. Advances in solid-state relaxation methodology for probing site-specific protein dynamics. *Acc. Chem. Res.* **46**, 2018–2027 (2013).
37. Trott, O. & Palmer, A. G. R1ρ Relaxation outside of the Fast-Exchange Limit. *J. Magn. Reson.* **154**, 157–160 (2002).
38. Baldwin, A. J. & Kay, L. E. An R1ρ expression for a spin in chemical exchange between two sites with unequal transverse relaxation rates. *J. Biomol. NMR* **55**, 211–218 (2013).
39. Öster, C. *et al*. Characterization of Protein–Protein Interfaces in Large Complexes by Solid-State NMR Solvent Paramagnetic Relaxation Enhancements. *J. Am. Chem. Soc.* **139**, 12165–12174 (2017).
40. Pratihar, S. *et al*. Kinetics of the Antibody Recognition Site in the Third IgG-Binding Domain of Protein G Zuschriften. *Angew. Chemie Int. Ed.* **55**, 9566–9569 (2016).
41. Lamley, J. M. *et al*. Unraveling the complexity of protein backbone dynamics with combined (13)C and (15)N solid-state NMR relaxation measurements. *Phys. Chem. Chem. Phys.* **17**, 21997–2008 (2015).
42. Gauto, D. F. *et al*. Protein conformational dynamics studied by 15 N and 1 H R 1ρ relaxation dispersion: Application to wild-type and G53A ubiquitin crystals. *Solid State Nucl. Magn. Reson.* **87**, 86–95 (2017).
43. Lange, O. F., Grubmüller, H. & De Groot, B. L. Molecular dynamics simulations of protein G challenge NMR-derived correlated backbone motions. *Angew. Chemie - Int. Ed.* **44**, 3394–3399 (2005).
44. Markwick, P. R. L., Bouvignies, G. & Blackledge, M. Exploring multiple timescale motions in protein GB3 using accelerated molecular dynamics and NMR spectroscopy. *J. Am. Chem. Soc.* **129**, 4724–4730 (2007).
45. Bouvignies, G. *et al*. Identification of slow correlated motions in proteins using residual dipolar and hydrogen-bond scalar couplings. *Proc. Natl. Acad. Sci.* **102**, 13885–13890 (2005).
46. Gronenborn, A. M. & Clore, G. M. Idenfication of the Contact Surface of a Streptococcal Protein G Domain Complexed with a Human Fc Fragment. *J. Mol. Biol.* **233**, 331–335 (1993).
47. Sauer-Eriksson, A. E., Kleywegt, G. J., Uhlén, M. & Jones, T. A. Crystal structure of the C2 fragment of streptococcal protein G in complex with the Fc domain of human IgG. *Structure* **3**, 265–278 (1995).
48. Zinkevich, T., Chevelkov, V., Reif, B., Saalwächter, K. & Krushelnitsky, A. Internal protein dynamics on ps to μs timescales as studied by multi-frequency 15N solid-state NMR relaxation. *J. Biomol. NMR* **57**, 219–235 (2013).

49. Krushelnitsky, A., Gauto, D., Rodriguez Camargo, D. C., Schanda, P. & Saalwächter, K. Microsecond motions probed by near-rotary-resonance R1ρ 15N MAS NMR experiments: the model case of protein overall-rocking in crystals. *J. Biomol. NMR* **71**, 53–67 (2018).
50. Vajpai, N., Gentner, M., Huang, J.-R., Blackledge, M. & Grzesiek, S. Side-chain chi(1) conformations in urea-denatured ubiquitin and protein G from (3)J coupling constants and residual dipolar couplings. *J. Am. Chem. Soc.* **132**, 3196–3203 (2010).
51. Franks, W. T. *et al.* Magic-angle spinning solid-state NMR spectroscopy of the beta-1 immunoglobulin binding domain of protein G (GB1): 15N and 13C chemical shift assignments and conformational analysis. *J. Am. Chem. Soc.* **127**, 12291–12305 (2005).
52. Lewandowski, J. R. *et al.* Measurement of site-specific 13C spin-lattice relaxation in a crystalline protein. *J. Am. Chem. Soc.* **132**, 8252–4 (2010).
53. Zhou, D. H. & Rienstra, C. M. High-performance solvent suppression for proton detected solid-state NMR. *J. Magn. Reson.* **192**, 167–72 (2008).
54. Clore, G. M., Driscoll, P. C., Wingfield, P. T. & Gronenborn, A. M. Analysis of the backbone dynamics of interleukin-1.beta. using two-dimensional inverse detected heteronuclear nitrogen-15-proton NMR spectroscopy. *Biochemistry* **29**, 7387–7401 (1990).

Acknowledgements

The research leading to these results has received funding from the European Research Council under the European Union's Seventh Framework Programme (FP/2007–2013)/ERC Grant Agreement 639907. J.R.L. also acknowledges funding from BBSRC Grant BB/L022761/1 and BB/R010218/1. C.Ö. acknowledges funding from the European Union under a Marie Curie Initial Training Network FP7-PEOPLE-2012-ITN Grant Agreement Number 316630 CAS-IDP. The UK 850 MHz solid-state NMR Facility used in this research was funded by EPSRC and BBSRC (contract reference PR140003), as well as the University of Warwick including via part funding through Birmingham Science City Advanced Materials Projects 1 and 2 supported by Advantage West Midlands (AWM) and the European Regional Development Fund (ERDF). We thank the 850 MHz Facility Manager, Dinu Iuga, for assistance in acquiring the data at the 850 MHz spectrometer. We thank Alexei Krushelnitsky for stimulating conversations, Paul Schanda for guidance with Gamma simulations and Ilya Kuprov for help with SPINACH simulations. Molecular graphics in Fig. 3 was generated in UCSF ChimeraX, developed by the Resource for Biocomputing, Visualization, and Informatics at the University of California, San Francisco, with support from NIH R01-GM129325 and P41-GM103311.

Author Contributions

C.Ö. and J.R.L. designed, performed and analyzed the experiments. S.K. has prepared protein samples. C.Ö., S.K. and J.R.L. and wrote the manuscript.

Additional Information

Supplementary information accompanies this paper at https://doi.org/10.1038/s41598-019-47507-8.

Competing Interests: The authors declare no competing interests.

Publisher's note: Springer Nature remains neutral with regard to jurisdictional claims in published maps and institutional affiliations.